PROCEEDINGS A

royalsocietypublishing.org/journal/rspa

Research

Check for updates

Article submitted to journal

Subject Areas:
xxxxx, xxxxx, xxxx

Keywords:
xxxx, xxxx, xxxx

Author for correspondence:
Jorge Viñals
e-mail: vinals@umn.edu

Biomechanics of orientationally ordered epithelial tissue

Patrick W. Alford[1], Luiza Angheluta[2] and Jorge Viñals[3]

[1]Department of Biomedical Engineering, University of Minnesota, Minneapolis, MN 55455
[2]Njord Centre, Department of Physics, University of Oslo, P.O. Box 1048, 0316 Oslo, Norway
[3]School of Physics and Astronomy, University of Minnesota, Minneapolis, MN 55455

Organogenesis involves large deformations and complex shape changes that require elaborate mechanical regulation. Models of tissue biomechanics have been introduced to account for the coupling between mechanical response and biochemical processes. Recent experimental evidence indicates that the mechanical response of epithelial tissue is strongly anisotropic, with the degree of anisotropy being correlated with the existence of long range orientational order of cytoskeletal organization across the tissue. A theoretical framework is introduced that captures the dynamic feedback between tissue elastic response and cytoskeletal reorganization under stress. Within the linear regime for small and uniform applied strains, the shear modulus is effectively reduced by the nematic order in cytoskeletal alignment induced by the applied strain. This prediction agrees with experimental observations of epithelial response in lithographically patterned micro tissues.

1. Introduction

A continuum theory is introduced that combines a model of cellular or fiber alignment with finite deformation elasticity to describe the biomechanics of epithelial tissue. Anisotropic mechanical response of tissue and its growth are known to correlate well with patterns of alignment, which in turn, respond to and are modified by applied traction.

THE ROYAL SOCIETY PUBLISHING

Our focus here is on the class of tissues that contain regular fibrous matrices in which the degree of fiber orientation induces anisotropic elastic response [1–5]. The recent recognition that long ranged alignment is present in a wide variety of tissues has prompted the extension of physical models of nematic order to cell biology [6], especially in the context of active matter in a nematic phase [7,8].

Nematic order refers to the existence of long range orientational correlations in the medium as described by an appropriately defined order parameter [9]. Two commonly used choices of order parameter include a director field, a unit vector $\hat{\boldsymbol{n}}$ that describes the local average of the predominant direction, and a tensor $\boldsymbol{Q}$ which we use below, defined as the second moment of the probability distribution function of orientations. The biological relevance of nematic order has been established in a number of different settings. Retinal morphogenesis and the development of the central nervous system in the zebra fish rely on the establishment of stratified epithelia which, in the proliferative phase, exhibit elongated shapes of the cell nuclei and nematic order [10]. Such nematic order is argued to act as a precursor during organogenesis, and to be a conserved feature of evolution. The healing of a wound in a layer of epithelial cells has been shown, both experimentally and theoretically, to be well modeled as an active nematic tissue [11]. Orientational order far or near the wound boundary differ, and contribute to active stresses and to boundary motion. The so called oncostreams are pathological structures in the brain comprising aligned spindle cells that also feature long ranged nematic order [12,13]. They are closely linked to glioma aggressiveness in the brain, and are believed to be key in the rapid spreading of tumors to the surrounding tissue, even after the main tumor is surgically removed. Oncostreams appear to feature overexpression of key genes that drive the epithelial to mesenchimal transition and lead to malignancy.

A central feature of nematic order is the existence of topological defects; small regions in which order is not defined [14]. While we do not address them explicitly in the study below, they appear as singular solutions to the same equations of motion that we present. Topological defects in nematics, called disclinations, have also been argued to have biological relevance [15]. For example, disclinations have been shown to act as organizing centers of growth in hydra [16]. Disclinations are accompanied by elastic gradients which are argued to be responsible for this particular mode of organogenesis. Cell death and extrusion have also been linked to nematic disclinations [17]. Defects are seen to produce spatially localized compressive stresses that are sufficiently intense to lead to cell response, death, and eventual extrusion from the tissue.

Significant evidence points more specifically towards the consequences of nematic order on cell mechanobiology [4,5,18–20]. Controlled experiments on lithographically patterned cells and micro tissues (both in vascular smooth muscle cells and in Madin–Darby canine kidney tissue (MDCK)) have revealed the effect of traction on fiber orientation, and the resulting modification to tissue stiffness and to its elastic anisotropy. The recently developed cellular micro-biaxial stretching system (CμBS) [4,5], coupled to traction force microscopy, produces the spatially resolved stress field during prescribed traction protocols. Confocal microscopy is then used to determine the point wise distribution of fiber orientation. The experiments show that the degree of cytoskeletal fiber orientation is itself a dynamical variable, exhibiting spatio temporal variation as the tissue remodels under imposed loads [4,5]. This observation, together with a measured change in tissue stiffness under stretching along the predominant direction of the fiber network, suggest response akin to a uniaxial solid (also known as a transverse isotropic solid), with both elastic distortion and fiber orientation coupled as dynamical fields. The description of this observed phenomenology is the main aim of the continuum theory introduced below.

Our starting point is the classical treatment of the cell (and of an extracellular matrix if present) as a continuum, elastic material [2,21,22]. More recent models have added some degree of cellular microstructural detail into improved constitutive laws by considering, for example, fiber orientation distributions to capture the anisotropic architecture of the cell, or of the extra cellular matrix surrounding the cells [23,24]. Of particular relevance to our study, is the introduction of the so called "anisotropy tensors" to account for structural cytoskeletal orientation within a

tissue [4,23,25–27]. Finite Element computational frameworks have been utilized to analyze the derived elastic response under a variety of conditions [4,28].

The main aim of our work below is the development of a thermodynamically consistent theory that combines finite deformation (nonlinear) elasticity, the evolution of orientational order as described by the nematic tensor order parameter $\boldsymbol{Q}$ and the concomitant tissue shape change, and tissue growth driven by imposed stresses (for example, in the form of cell proliferation). We introduce a dissipation inequality for a free energy that is a functional of elastic and alignment fields, but not of the tensor introduced to describe growth. Unlike classical biomechanics treatments that factorize the deformation gradient tensor into elastic and growth components [29], we suggest that the growth tensor is not a proper thermodynamic variable, rather a kinetic effect that needs to be treated separately. We note, however, that the growth tensor formulation has yielded significant contributions in studies of embriogenesis, morphogenesis, and the description of various pathologies (wound healing, fibrosis, and tumorgenesis and metastasis) [29,30]. In the small deformation limit, both approaches are equivalent in terms of elastic response, but they are not when considering dissipation or nonlinear elasticity. We extend here the classical formulation based on the growth tensor to include a different (kinematic) definition, and its dependence on the local state of orientation in the tissue.

The development of a theory of tissue biomechanics along the lines described above, necessitates validation against benchmark experiments, as well as a determination of the values of the elastic and growth parameters that it contains for each specific tissue. The theory needs to include three widely distinct time scales associated with three phenomena at play: Elastic response (essentially instantaneous), actin polimerization and fiber network remodeling (on a scale of seconds), and cell proliferation, also in response to stresses (on a scale of hours). We present a comparison between the theory and experiments on micro contact printed tissue in the recently developed Cellular, Microbiaxial Stretching system (CμBS), combined with traction force and confocal microscopies [5]. While still preliminary as the experiments available were not designed to test the theory, we find that early time fiber reorientation under traction as measured in MDCK tissue, is consistent with the theory, and we obtain the value of the key coupling coefficient between distortion and alignment. More complex traction protocols will be designed and implemented on the CμBS in the future that will allow a more complete validation.

We finally note that while our primary motivation here is modeling the biomechanics of epithelial tissue, the same model and thermodynamic description presented can be used to understand other nanotechnology and materials science systems that rely on bio inspired design of artificial tissue. For example, myosin, a nanoscale motor protein that controls cell shape, can be used to produce on demand contractile, shape adaptive materials [31]. Artificial tissue can also be used as a platform for the investigation of physical phenomena, such as bistability, oscillation, wave propagation, and excitability. Classic plastic flow has been argued to occur in models of tissue [32]. A yet different class of studies focus on self-healing materials relying, in part, in lessons from their biological counterparts [33]. The formulation presented below is not restricted to small deformations, and hence could be used to describe materials in which large changes of shape occur when coupled to orientational order.

2. Transport model

We consider a deformed tissue described by a displacement vector $\boldsymbol{u} = \boldsymbol{x} - \boldsymbol{X}$ where $\boldsymbol{x} = \{x_i\}$ are the coordinates in the deformed state, relative to reference state $\boldsymbol{X} = \{X_i\}$. In terms of the displacement field $\boldsymbol{u}$ (which exists in the compatible case), the distortion tensor is defined as $U_{ij} = \partial u_i/\partial x_j = \delta_{ij} - F^{-1}_{ij}$. We will denote $\partial_i = \partial/\partial x_i$, the derivative in the current configuration. The tensor $F_{ij} = \frac{\partial x_i}{\partial X_j}$ is the deformation gradient tensor, the Jacobian matrix of the coordinate transformation. Its inverse is a direct measure of the distortion, which is the primary quantity of interest below. We define $\boldsymbol{W} = \boldsymbol{F}^{-1}$, the inverse of the elastic deformation tensor. The local state of a tissue is assumed to depend on $\boldsymbol{W}$.

In order to characterize the local state of fiber orientation, one can introduce the so called nematic director field, a unit vector $\hat{\boldsymbol{n}}(\mathbf{x})$ that gives the local statistical average of the orientation of the fibers [9,34]. Figure 2 shows a bright field image of a patterned micro tissue stained for its F-actin network, together with the predominant fiber orientation $\hat{\boldsymbol{n}}(\mathbf{x})$. The figure also shows the distribution of fiber orientations, for three different tissue patterns and state of elongation (see Ref. [5] for details and protocols). The director only determines direction, and hence the orientation distribution is invariant under $\hat{\boldsymbol{n}} \to -\hat{\boldsymbol{n}}$. An alternative representation of orientational order is the nematic tensor order parameter $\boldsymbol{Q}(\boldsymbol{x})$ which gives *both* the magnitude and direction of local fiber orientation. If $p(\boldsymbol{\xi})$ is the local distribution of fiber orientation, the tensor $\boldsymbol{Q}$ is defined in terms of the average

$$\boldsymbol{Q} = \int_{\mathcal{S}^2} d\Sigma \, (\frac{3}{2}\boldsymbol{\xi} \otimes \boldsymbol{\xi} - \frac{1}{2}\boldsymbol{I}) p(\boldsymbol{\xi})$$

The domain of integration is the unit sphere $\mathcal{S}^2$, with surface element $d\Sigma$. By definition the tensor $\boldsymbol{Q}$ is symmetric and traceless. $\boldsymbol{Q}$ may be diagonalized with real eigenvalues, $\lambda_1 \geq \lambda_2 \geq \lambda_3$, and corresponding orthonormal eigenvectors , $\hat{\boldsymbol{n}}$, $\hat{\boldsymbol{m}}$, $\hat{\boldsymbol{l}}$. The scalar uniaxial order parameter (the measure of uniaxial order) may be defined as $S = \lambda_1$ [35]. In this definition, S is positive everywhere, even at disclination cores (in the so called pancake configuration).

Under isothermal conditions, the free energy of a deformed body with some degree of nematic order is written as

$$\mathcal{F}\left[\boldsymbol{W}(\boldsymbol{x},t), \boldsymbol{Q}(\boldsymbol{x},t), \nabla\boldsymbol{Q}(\boldsymbol{x},t)\right] = \int_{\Omega} dV \; \rho f \left(\boldsymbol{W}(\boldsymbol{x},t), \boldsymbol{Q}(\boldsymbol{x},t), \nabla\boldsymbol{Q}(\boldsymbol{x},t)\right), \tag{2.1}$$

where ρ is the mass density, and f the free energy per unit mass. The free energy can be written as
$f\left(\boldsymbol{W}(\boldsymbol{x},t), \boldsymbol{Q}(\boldsymbol{x},t), \nabla\boldsymbol{Q}(\boldsymbol{x},t)\right) = f_{el}(\boldsymbol{W}(\boldsymbol{x},t), \boldsymbol{Q}(\boldsymbol{x},t)) + f_n(\boldsymbol{Q}(\boldsymbol{x},t), \nabla\boldsymbol{Q}(\boldsymbol{x},t))$, the sum of an elastic contribution f_{el} dependent on distortion, and a nematic contribution f_n. Since the tissue in its actual, deformed state, presents orientational order, $f_{el}(\boldsymbol{W}(\boldsymbol{x},t), \boldsymbol{Q}(\boldsymbol{x},t))$ is that of a uniaxial (or transversely isotropic) solid [36,37]. We take the nematic contribution to be of the Landau-de Gennes form [9,34],

$$\rho f_n = \frac{1}{2}K|\nabla\boldsymbol{Q}|^2 - \frac{a}{2}\mathrm{Tr}(\boldsymbol{Q}^2) - \frac{b}{3}\mathrm{Tr}(\boldsymbol{Q}^3) + \frac{c}{4}\left(\mathrm{Tr}(\boldsymbol{Q}^2)\right)^2 \tag{2.2}$$

where K, a, b, c are material parameters and positive. Minimizers of f_n in the absence of distortion are either uniaxial or isotropic $\boldsymbol{Q}$ tensors.

Consider now a dissipation inequality according to which the work done by external forces on the body $\Omega(t)$ (the actual body, which is distorted) has to be larger that the rate of change of its free energy plus the kinetic energy. We do not consider below the work done on the external boundary by a time dependent $\boldsymbol{Q}$ tensor on the boundary (see [34] for an analysis of this contribution). We assume that the tensor $\boldsymbol{Q}$ is independent of time on the body boundary. The dissipation inequality reads,

$$\int_{\partial\Omega} (\boldsymbol{T}\cdot\boldsymbol{n})\cdot\boldsymbol{v}\, dS \geq \frac{d}{dt}\int_{\Omega}\rho f dV + \frac{d}{dt}\int_{\Omega}\frac{1}{2}\rho v^2 dV \tag{2.3}$$

where $\boldsymbol{T}$ is the Cauchy stress tensor, $\boldsymbol{n}$ the unit normal at $\partial\Omega$, the boundary of the body, ρ is the mass density, $\boldsymbol{v}$ the local center of mass velocity. In components, contractions follow the convention $T_{ij}\partial_j v_i = \boldsymbol{T} : \nabla\boldsymbol{v} = \boldsymbol{T} : \boldsymbol{L}$, where in the velocity gradient tensor $L_{ij} = \partial_j v_i$, both velocity and derivatives are spatial, that is, in the actual, deformed body. Standard manipulations using the divergence theorem and the momentum balance $\rho\dot{\boldsymbol{v}} = \nabla\cdot\boldsymbol{T}$, lead to [38,39]

$$\int_{\partial\Omega} (\boldsymbol{T}\cdot\boldsymbol{n})\cdot\boldsymbol{v}\, dS = \frac{d}{dt}\int_{\Omega}\frac{1}{2}\rho v^2 dV + \int_{\Omega}\boldsymbol{T}:\boldsymbol{L}\, dV$$

such that the energy dissipation inequality reduces to

$$\int_{\Omega} dV \left[\boldsymbol{T}:\boldsymbol{L} - \frac{d}{dt}(\rho f) - (\rho f)\mathrm{Tr}(\boldsymbol{L})\right] \geq 0, \tag{2.4}$$

where the last term comes from volume change.

Up to this point, no dependence of the free energy on growth is assumed. However, in order to compute the time derivative of the free energy density, we need a kinematic law for $\boldsymbol{W}$. This kinematic law needs to incorporate both elastic distortion of the tissue, as well as its anelastic deformation due to remodeling and cell proliferation. The traditional route (see, e.g., Ref. [29]) is to multiplicatively decompose the tensor $\boldsymbol{F}$ into elastic and growth contributions, $\boldsymbol{F} = \boldsymbol{F}^{el}\boldsymbol{G}$, where $\boldsymbol{G}$ is the so called growth tensor. Because $\boldsymbol{F}$ is a two point tensor, this definition implies the need to define $\boldsymbol{G}$ in an unobservable, and non unique reference configuration of fiber orientation. We follow an alternative approach recently developed for the theory of thermo plasticity that does not rely on this multiplicative decomposition [40]. One starts from the well accepted additive decomposition of the spatial velocity gradient into an elastic and a growth part,

$$\dot{\boldsymbol{W}} + \boldsymbol{W}\boldsymbol{L} = \boldsymbol{Y}\dot{\boldsymbol{G}} \tag{2.5}$$

where $\boldsymbol{Y}$ is a two point tensor to be determined, and $\dot{\boldsymbol{G}}$ is the growth rate tensor now defined in the actual state. Invariance under rotation of Eq. (2.5) implies that $\boldsymbol{Y}$ must transform as $\boldsymbol{W}$ under rotation, provided that $\dot{\boldsymbol{G}}$ is a symmetric tensor. The simplest approximation is to take them proportional to each other, with a scalar function factor. This scalar function will enter multiplicatively in the Onsager coefficients of the dissipation analysis later, so for now we just take $\boldsymbol{Y} = \boldsymbol{W}$. The kinematic law for the inverse elastic distortion is therefore,

$$\dot{\boldsymbol{W}} + \boldsymbol{W}\boldsymbol{L} = \boldsymbol{W}\dot{\boldsymbol{G}} \tag{2.6}$$

This implies that the spatial velocity gradient is $\boldsymbol{L} = -\boldsymbol{W}^{-1}\dot{\boldsymbol{W}} + \dot{\boldsymbol{G}}$

The material time derivative of the free energy density leads to,

$$\int_\Omega dV \left\{ \boldsymbol{T} : \boldsymbol{L} - \left[\frac{\partial(\rho f)}{\partial \boldsymbol{W}} : \dot{\boldsymbol{W}} + \rho f \mathrm{Tr}(\boldsymbol{L}) + \frac{\partial(\rho f)}{\partial \boldsymbol{Q}} : \dot{\boldsymbol{Q}} + \frac{\partial(\rho f)}{\partial(\nabla \boldsymbol{Q})} \vdots \dot{(\nabla \boldsymbol{Q})} \right] \right\} \geq 0, \tag{2.7}$$

where $\dot{\boldsymbol{W}}$ is given in Eq. (2.5), and the triple dot is a triple index contraction. Concerning the last term in the right hand side, we note the material time derivative and the partial spatial derivative do not commute. If φ is a scalar function, or a component of a vector or tensor, one has [41] $\partial_i(\dot{\varphi}) = \dot{(\partial_i \varphi)} + (\partial_i v_j)(\partial_j \varphi)$. The $\boldsymbol{Q}$ tensor derivative reads [42],

$$\dot{(\partial_k Q_{ij})} = \partial_k(\dot{Q}_{ij}) - (\partial_k v_l)(\partial_l Q_{ij})$$

The dissipation inequality now reads,

$$\int_{\Omega(t)} dV \left\{ \left[T_{ij} + \frac{\partial(\rho f)}{\partial W_{mi}} W_{mj} - \rho f \delta_{ij} + \frac{\partial(\rho f)}{\partial(\partial_j Q_{mn})} (\partial_i Q_{mn}) \right] \partial_j v_i \right.$$
$$\left. - \int_{\Omega(t)} dV \, \frac{\partial(\rho f)}{\partial W_{ij}} W_{ik} \dot{G}_{ik} - \int_{\Omega(t)} dV \, h_{ij} \dot{Q}_{ij} \right\} \geq 0,$$

where the molecular field h_{ij} is the conjugate of Q given the free energy Eq. (2.1), and it is given by

$$(\boldsymbol{H})_{ij} = h_{ij} = \frac{\delta \mathcal{F}}{\delta Q_{ij}} = \frac{\partial(\rho f)}{\partial Q_{ij}} - \partial_k \frac{\partial(\rho f)}{\partial(\partial_k Q_{ij})}. \tag{2.8}$$

We have used integration by parts and that fact that the tensor $\boldsymbol{Q}$ is independent of time on the boundary.

One considers first reversible motion in which the equality holds: $\dot{\boldsymbol{Q}} = 0$ and $\dot{\boldsymbol{G}} = \alpha \dot{\boldsymbol{Q}} = 0$, so that the nematic and growth tensors are simply transported by the distortion. We also take the first terms in square brackets to be zero, leading naturally to the Ericksen stress, the reversible

component of the stress,

$$T^R_{ij} = T^E_{ij} = -\frac{\partial(\rho f)}{\partial W_{mi}} W_{mj} - \frac{\partial(\rho f)}{\partial(\partial_j Q_{mn})} \partial_i Q_{mn} + \rho f \delta_{ij}. \tag{2.9}$$

The second term is the analog of the capillary stress $\frac{\partial f}{\partial(\partial_i \psi)} \partial_j \psi$ for a scalar order parameter ψ in the Cahn-Hilliard fluid theory [41].

Consideration of dissipative currents in general is quite complicated, as already given in nematic liquid crystals in Refs. [43,44] and [45] for nonlinear elasticity. We follow a simpler approach that can be justified by the disparity in time scales between the elastic response of the tissue, tissue shape remodeling, and cell proliferation in response to stresses. Such as disparity is clearly evidenced by traction force microscopy experiments in single cell tissue [4], and in patterned microtissue [5]. Therefore we adopt a quasistatic approximation according to which the material is in elastic equilibrium compatible with the instantaneous conditions of fiber orientation and cell number, $\nabla \cdot \boldsymbol{T}^R = 0$. Therefore the computation of independent velocities is not necessary as the tissue deforms according to the instantaneous displacement. The same property applies to the transport of nematic order and growth tensor. In order to develop a computational method, we note that the center of mass velocity (for compatible motion) $\mathbf{v} = \dot{\mathbf{u}}$. The equation of elastic equilibrium can be re written as $\partial_j \dot{T}_{ij} = \partial_j(\partial_t T_{ij} + v_k \partial_k T_{ij}) = 0$ since $\partial_j T_{ij} = 0$. Therefore the equation of elastic equilibrium can be written in terms of the velocities as well as $\nabla \cdot \dot{\boldsymbol{T}} = 0$. We do not include viscous dissipation in the momentum balance equation.

One can still consider dissipation in the slower scale motion of $\dot{\boldsymbol{Q}}$ and $\dot{\boldsymbol{G}}$. Note that the growth term in the dissipation inequality can be written as $\int_{\Omega(t)} d\boldsymbol{x}\, \boldsymbol{\sigma} : \dot{\boldsymbol{G}}$ where the elastic Cauchy stress tensor is defined here as $\boldsymbol{\sigma} = -\boldsymbol{W}^T \frac{\partial(\rho f)}{\partial \boldsymbol{W}}$. This is the contribution to dissipation due to growth under stress. $\boldsymbol{G}$ is a second rank tensor, and therefore since both $\boldsymbol{Q}$ and $\boldsymbol{G}$ also have the same signature under time reversal, they can couple dissipatively (Curie principle). In the simplest, isotropic, case, we write for the dissipative rates,

$$\dot{\boldsymbol{G}}^D = \gamma \boldsymbol{\sigma} - \gamma' \left[\frac{\delta \mathcal{F}}{\delta \boldsymbol{Q}}\right]_{tr} \tag{2.10}$$

$$\dot{\boldsymbol{Q}}^D = -\Gamma \left[\frac{\delta \mathcal{F}}{\delta \boldsymbol{Q}}\right]_{tr} - \gamma' \left[\boldsymbol{\sigma}\right]_{tr}, \tag{2.11}$$

where $[.]_{tr}$ denotes the traceless part of the tensor, $\dot{\boldsymbol{Q}}^D = \dot{\boldsymbol{Q}} - \dot{\boldsymbol{Q}}^R$, and $\dot{\boldsymbol{G}}^D = \dot{\boldsymbol{G}} - \dot{\boldsymbol{G}}^R$, are the total rates minus the reversible components. The coefficients $\Gamma, \gamma, \gamma' > 0$. The tensor of Onsager coefficients in each equation have been simplified to scalars. Recall that γ can be a scalar function of position as we have absorbed here the undetermined scalar function factor in the definition of $\boldsymbol{Y}$.

3. Small deformation and isotropic medium

In order to illustrate a few properties of our model, and to present a comparison with the experiments of Ref. [5], discussed in Sec. 4, we consider the limit of small deformation $\boldsymbol{W} = \boldsymbol{F}^{el,-1} = (\boldsymbol{I} + \boldsymbol{U}^{el})^{-1} \approx \boldsymbol{I} - \boldsymbol{U}^{el}$. In this limit, the kinetic law $\dot{\boldsymbol{W}} + \boldsymbol{W}\boldsymbol{L} = \boldsymbol{W}\dot{\boldsymbol{G}}$ can be written (to first order in all quantities) as $\nabla \dot{\boldsymbol{u}} = \dot{\boldsymbol{U}}^{el} + \dot{\boldsymbol{G}}$. Since $\boldsymbol{W}$ is compatible, we have simply replaced $\dot{\boldsymbol{u}} = \boldsymbol{v}$ in $\boldsymbol{L}$. This equation can be integrated over time, yielding (a time independent distortion as the constant of integration is omitted),

$$\nabla \boldsymbol{u} = \boldsymbol{U}^{el} + \boldsymbol{G} \tag{3.1}$$

Note that no assumption about the multiplicative decomposition of the deformation tensor is necessary for this additive decomposition to hold. In small deformation, the symmetrized distortion is the linear strain, so that we write $\boldsymbol{\varepsilon} = \boldsymbol{\varepsilon}^{el} + \boldsymbol{G}$. The tensor $\boldsymbol{G}$ needs to be symmetric for the decomposition (2.5) to hold.

Tissue is approximately elastically incompressible, and the analysis of Sec. 4 concerns the response at early times following the imposed stretch, before the onset of any appreciable cell proliferation. Also, and for the purpose of the estimate, we assume that the tissue is elastically isotropic. Under both assumptions, the elastic free energy is $f_{el} = \mu \boldsymbol{\varepsilon}^{el} : \boldsymbol{\varepsilon}^{el}$. Therefore,

$$\boldsymbol{T}^R = 2\mu\,(\boldsymbol{\varepsilon} - \alpha \boldsymbol{Q}) + K \nabla \boldsymbol{Q} \odot \nabla \boldsymbol{Q}. \tag{3.2}$$

The product in the last term in the right hand side is defined as $(\partial_\alpha Q_{ij} \partial_\beta Q_{ij})_{\alpha,\beta=1,3}$, with the components of $\boldsymbol{Q}$ contracted over. We note that the corrections to the stress is the same as that for a nematic elastomer [37]. A local change in nematic order induces elastic (reversible) distortion, which in turn modifies the elastic response ("soft elasticity ") (the coefficient α can be positive or negative depending on the material). The last term is the well known Ericksen stress in liquid crystals, which arises directly from nematic elasticity.

The equation of motion for the $\boldsymbol{Q}$ tensor follows from Eq. (2.11), together with $f_{el} = \mu(\boldsymbol{\varepsilon} - \alpha\boldsymbol{Q}) : (\boldsymbol{\varepsilon} - \alpha\boldsymbol{Q})$ and f_n in Eq. (2.2),

$$\dot{Q}_{ij} = 2\mu\alpha\Gamma(\varepsilon_{ij} - \alpha Q_{ij}) + \Gamma\left[K\nabla^2 + a - c\mathrm{Tr}(\boldsymbol{Q}^2)\right] Q_{ij} + \Gamma b Q_{ik} Q_{kj} \tag{3.3}$$

where we have also neglected the cross coupling coefficient for the dissipative evolution of the tensor order parameter.

(a) Steady state under a uniform stretch

To examine more closely the feedback between nematic order and elasticity, we solve for the steady state resulting from a small perturbation $\|\delta\boldsymbol{Q}\| \ll 1$ relative to the equilibrium nematic order $\boldsymbol{Q}^{(0)}$ with $\|\boldsymbol{Q}^{(0)}\| = Q_0$ at zero stress, which the magnitude $Q_0 = \sqrt{a/c}$. Thus, the reference state with uniform nematic $Q_{ij}^{(0)}$ corresponds to $T_{ij}^{R0} = \varepsilon_{ij}^{(0)} = 0$. We also neglect cell proliferation as a source of deformation ($\mathrm{Tr}(\boldsymbol{L}) = 0$). In a time scale of seconds to minutes, the medium can be taken as effectively incompressible.

For a system in three dimensions, the nematic tensor order parameter for a uniaxial state can be written as [9] $Q_{ij} = S(\frac{3}{2} n_i n_j - \frac{1}{2}\delta_{ij})$, where the unit vector $\hat{\mathbf{n}}$ is the uniaxial director, and S is the degree of uniaxial order. This definition is consistent with the definition of the structure tensor in Ref. [23], except that the $\mathbf{Q}$ tensor is made traceless. An orientationally disordered system has $S = 0$, whereas the perfectly oriented case has $S = 1$. In order to compare our results with existing data on thin films of patterned micro-tissue (Sec. 4), the analogous definition of the tensor order parameter in two dimensions is $Q_{ij} = S(2\hat{n}_i\hat{n}_j - \delta_{ij})$. In this case, $\mathrm{Tr}(\boldsymbol{Q}^3) = 0$, the cubic term in the free energy functional (2.2) and its corresponding term in the evolution of $\mathbf{Q}$ from Eq. (3.3) do not appear in two dimensions.

Let us now consider a uniformly perturbed state $\delta\boldsymbol{Q}$, $\delta\boldsymbol{T}^R$ due to an applied (uniform) strain $\delta\boldsymbol{\varepsilon}$. The relation between these perturbations is

$$\delta T_{ij}^R \quad = \quad 2\mu(\delta\varepsilon_{ij} - \alpha\delta Q_{ij}).$$

To find the steady state equation for $\boldsymbol{Q}$ tensor equation, we need to linearize the cubic term,

$$\begin{aligned}
\mathrm{Tr}(\boldsymbol{Q}^2)Q_{ij} &= Q_{kl}Q_{kl}Q_{ij} = \\
(Q_{kl}^{(0)} + \delta Q_{kl})(Q_{kl}^{(0)} + \delta Q_{kl})Q_{ij} &= (Q_0^2 + \delta Q_{kl}Q_{kl}^{(0)} + Q_{kl}^{(0)}\delta Q_{kl} + \mathcal{O}(\delta Q^2))(Q_{ij}^{(0)} + \delta Q_{ij}) \\
&= (\delta Q_{kl}Q_{kl}^{(0)} + Q_{kl}^{(0)}\delta Q_{kl})Q_{ij}^{(0)} + Q_0^2\delta Q_{ij} + \mathcal{O}(\delta Q^2)
\end{aligned}$$

Thus, the equation for $\delta\boldsymbol{Q}$ follows as

$$c(\delta Q_{kl}Q_{kl}^{(0)} + Q_{kl}^{(0)}\delta Q_{kl})Q_{ij}^{(0)} = 2\alpha\mu\delta\varepsilon_{ij}, \tag{3.4}$$

using that $Q_0^2 = S_0^2 = a/c$. Notice that the perturbation depends both on the magnitude and the orientation of the reference nematic field relative to the applied strain. We write the equation

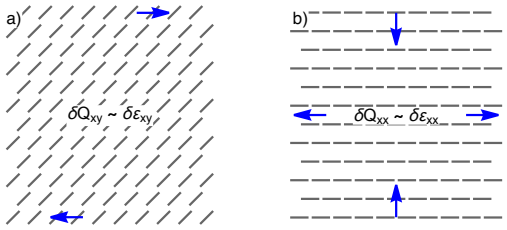

Figure 1: Steady state orientation of the nematic director for a) simple shear from Eq. 3.8 and for b) uniaxial strain from Eq. 3.7.

above for the two independent components δQ_{xx} and δQ_{xy}. First, we evaluate

$$\begin{aligned}\delta Q_{kl}Q^{(0)}_{kl} &= \delta Q_{xx}Q^{(0)}_{xx} + \delta Q_{xy}Q^{(0)}_{xy} + \delta Q_{yx}Q^{(0)}_{yx} + \delta Q_{yy}Q^{(0)}_{yy} \\ &= 2(\delta Q_{xx}Q^{(0)}_{xx} + \delta Q_{xy}Q^{(0)}_{xy})\end{aligned}$$

Thus,

$$\delta Q_{kl}Q^{(0)}_{kl} + Q^{(0)}_{kl}\delta Q_{kl} = 4(Q^{(0)}_{xx}\delta Q_{xx} + Q^{(0)}_{xy}\delta Q_{xy})$$

Hence, the two coupled equations read,

$$\begin{aligned}(Q^{(0)}_{xx})^2\delta Q_{xx} + Q^{(0)}_{xx}Q^{(0)}_{xy}\delta Q_{xy} &= \frac{\alpha\mu}{2c}\delta\varepsilon_{xx} \\ Q^{(0)}_{xx}Q^{(0)}_{xy}\delta Q_{xx} + (Q^{(0)}_{xy})^2\delta Q_{xy} &= \frac{\alpha\mu}{2c}\delta\varepsilon_{xy}\end{aligned}$$

We use a parameterization of $\boldsymbol{Q}$ in terms of the nematic director orientation, $\hat{\boldsymbol{n}} = [\cos(\theta); \sin(\theta)]$, namely that $Q_{xx} = S\cos(2\theta), \quad Q_{xy} = S\sin(2\theta)$, and arrive at the linear system

$$\underbrace{\begin{pmatrix}\cos^2(2\theta_0) & \sin(2\theta_0)\cos(2\theta_0) \\ \sin(2\theta_0)\cos(2\theta_0) & \sin^2(2\theta_0)\end{pmatrix}}_{A(\theta_0)}\begin{pmatrix}\delta Q_{xx} \\ \delta Q_{xy}\end{pmatrix} = \frac{\alpha\mu}{2cS_0^2}\begin{pmatrix}\delta\varepsilon_{xx} \\ \delta\varepsilon_{xy}\end{pmatrix}$$

This system is degenerate i.e. $\det[A(\theta_0)] = 0$ for any equilibrium nematic orientation θ_0. Since, rank(A)=1, a solution exists only when strain perturbation vector $[\delta\varepsilon_{xx}, \delta\varepsilon_{xy}]$ lies in the image of A corresponding to satisfying the compatibility condition

$$\frac{\delta\varepsilon_{xy}}{\delta\varepsilon_{xx}} = \tan(2\theta_0), \tag{3.5}$$

which implies that the strain perturbations depend on the equilibrium nematic orientation. Then, the system reduces to a single equation

$$\cos(2\theta_0)\delta Q_{xx} + \sin(2\theta_0)\delta Q_{xy} = \frac{\alpha\mu}{2cS_0^2}\left[\cos(2\theta_0)\delta\varepsilon_{xx} + \sin(2\theta_0)\delta\varepsilon_{xy}\right]. \tag{3.6}$$

There are two reference nematic orientations θ_0 for which these perturbations decouple:

a) $\theta_0 = 0$ implies that $\delta\varepsilon_{xy} = 0$ and $\delta\varepsilon_{xx}$ is unconstrained. The solution for this uniaxial (compression/extension) along the x direction corresponds to the nematic perturbation aligned with x,

$$\delta Q_{xx} = \frac{\alpha\mu}{2cS_0^2}\delta\varepsilon_{xx}, \qquad \delta T^R_{xx} = 2\mu\left(1 - \frac{\alpha^2}{2cS_0^2}\right)\delta\varepsilon_{xx}. \tag{3.7}$$

which is also shown in Fig. 1 a).

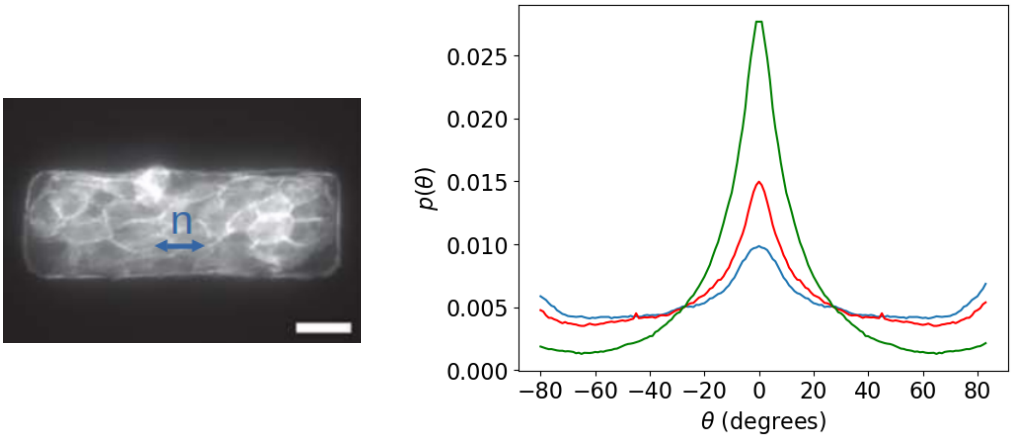

Figure 2: Left: Bright field image of MDCK tissue patterned in a rectangular shape (2:1 aspect ratio) showing its F-actin network. The predominant orientation along the x axis (left to right) is denoted by the director $\hat{\mathbf{n}}$. Right: Distribution of fiber orientation $p(\theta)$, with orientation relative to the x axis. Shown are the distributions for aspect ratio 1:1 (blue), aspect ratio 2:1 (red), and aspect ratio 2:1 under a 23% uniaxial strain along the x direction (green). The respective order parameters are $S = 0.41, 0.50$ and 0.75.

b) $\theta_0 = \pm\pi/4$ corresponds $\delta\varepsilon_{xx} = 0$ and $\delta\varepsilon_{xy}$ unconstrained. Thus, the allowed perturbation for this equilibrium nematic orientation is a pure shear which induces a nematic perturbation aligned with the shearing direction along x

$$\delta Q_{xy} = \frac{\alpha\mu}{2cS_0^2}\delta\varepsilon_{xy}, \quad \delta T^R_{xy} = 2\mu\left(1 - \frac{\alpha^2}{2cS_0^2}\right)\delta\varepsilon_{xy}, \tag{3.8}$$

as also shown in Fig. 1 b). For both of this cases, the applied strain acts to reinforce the nematic alignment by inducing perturbations δQ_{xx} and δQ_{xy} that are consistent with the orientation θ_0, thereby enhancing the magnitude of the nematic order. In general, when $\theta_0 \neq 0$ or $\pm\pi/4$, there is a family of solutions given by

$$\begin{pmatrix}\delta Q_{xx}\\ \delta Q_{xy}\end{pmatrix} = \frac{\alpha\mu}{2cS_0^2}\,\delta\varepsilon_{xx}\begin{pmatrix}1\\ \tan(2\theta_0)\end{pmatrix} + \lambda\begin{pmatrix}-\sin(2\theta_0)\\ \cos(2\theta_0)\end{pmatrix}, \quad \lambda\in\mathbb{R}.$$

4. Discussion and conclusions

We contrast here the results of Sec. 3 with experiments designed to probe the elastic response of micro patterned tissue (Madin–Darby canine kidney tissue, or MDCK) in the recently developed cellular micro-biaxial stretching system (CμBS) [5]. Rectangular, thin tissues were fabricated with a variety of aspect ratios, and stretched under controlled conditions. Internal stresses were determined by in situ traction force microscopy, and fiber orientation distributions measured by confocal microscopy in tissue stained for F-actin. The results corresponding to two particular aspect ratios are examined here: A square (1:1) micro tissue which is seen to be largely unoriented, and responds as an elastically isotropic medium, and a rectangular (2:1) tissue which displays significant nematic order along the long direction, order that changes under the stretching protocols [5].

Figure 2 shows the measured orientation distribution following the protocol of Ref. [5]. Shown are two control distributions for aspect ratios 1:1 (blue) and 2:1 (red), and then the distribution when the tissue has been stretched by 23% along the x direction (parallel to the director). Orientation increases significantly. The uniaxial order parameter can be computed as

$S = \langle \frac{3}{2}(\cos\theta)^2 - \frac{1}{2} \rangle$, where the average is taken over the measured distribution $p(\theta)$. We find $S = 0.41$ for 1:1 aspect ratio, $S = 0.50$ for 2:1 aspect ratio but no strain, and, $S = 0.75$ for 2:1 under uniaxial strain. Therefore $\delta Q_{xx} = \delta S = 0.25$.

The strain reported in the experiments is $\delta\varepsilon_{xx} = 0.23$. The resulting stress change δT^R_{xx} is more difficult to obtain as the experimental results (Fig. 9 of [5]) consider long duration runs of 24 hours, while tissue stretching per se only took 15s. During the remainder of the experiment cell proliferation dominates the deformation response. We therefore estimate the stress from the discontinuities at zero time shown in Fig. 9C (AR1 or 1:1 aspect ratio) and Fig. 9E (AR2, or 2:1 aspect ratio) in [5]. First, for that 1:1 sample, we estimate $\delta T_{xx} \approx 0.20kPa$ which yields an estimate of the shear modulus $\mu \approx 0.54kPa$ for for the assumed isotropic medium. This is within range of the known Young modulus of MDCK [46]. In the oriented case, we estimate $\delta T^R_{xx} \approx 0.17kPa$. From Eqs. (3.7), we obtain $\alpha \approx 0.16$.

The estimates just given have to be considered as preliminary, as they assume spatially uniform distributions of fiber orientational order and strain. However, in the case of the CμBS experiments of Ref. [5], an analysis of spatially resolved traction force microscopy reveals highly nonuniform distributions of stresses both in the isotropic AR1 and oriented AR2 tissues. Figure 4, for example, shows that the local values of tissue stress range from almost zero to 350 kPa. These local variations are of the same order as the tissue average values reported, which have been used in the estimates above.

Nevertheless, the calculations presented are consistent with the reduction in shear modulus observed in the experiments: To the extent that this reduction can be thought of as elastomeric in origin, the reduction has been argued to be of order μ [47,48], or α of order one, as we have estimated.

The results discussed serve as a preliminary feasibility test of the theory. We are currently undertaking more detailed, and early time experiments with different stretching protocols to isolate contributions from uniaxial elasticity, nematic order relaxation, and dissipation from cell proliferation, Eq. (2.10). Clearly, the longitudinal stiffness of actin fibers must contribute to the elastic response of an oriented micro tissue (see, e.g., the analysis in Ref. [4] for a single cell), a contribution not taken into account in our expansion around an elastically isotropic medium. Biaxial stretching can also be used to probe the prediction for the other steady state, case (b) in Sec. 3(a). And stretching transverse to the nematic director does not have an associated stationary solution, rather it will result in fiber reorientation. Finally, numerical computation will be necessary to compare the evolution of spatially resolved stresses, already available in Ref. [5], with predicted tissue growth.

Acknowledgements. We are indebted to Amit Acharya of Carnegie Mellon for many useful and stimulating discussions. This collaboration is supported by the Norwegian Centennial Chair Program, which is jointly funded by the Government of Norway and the University of Minnesota Foundation. The research of PA is supported by the National Science Foundation, contract CMMI 2230435, and JV by DMR 2223707.

References

1. Sacks MS, Sun W. 2003 Multiaxial mechanical behavior of biological materials. *Annual review of biomedical engineering* **5**, 251–284.
2. Humphrey J, Strumpf R, Yin F. 1990 Determination of a constitutive relation for passive myocardium: I. A new functional form. *ASME J. Biomech. Eng.* **112**, 333.
3. Kim DH, Lipke EA, Kim P, Cheong R, Thompson S, Delannoy M, Suh KY, Tung L, Levchenko A. 2010 Nanoscale cues regulate the structure and function of macroscopic cardiac tissue constructs. *Proceedings of the National Academy of Sciences* **107**, 565–570.
4. Win Z, Buksa JM, Steucke KE, Gant Luxton G, Barocas VH, Alford PW. 2017 Cellular microbiaxial stretching to measure a single-cell strain energy density function. *Journal of biomechanical engineering* **139**, 071006.
5. Cook BL, Alford PW. 2023 Continuum interpretation of mechano-adaptation in micropatterned epithelia informed by in vitro experiments. *Integrative Biology* **15**, zyad009.

6. Doostmohammadi A, Ladoux B. 2022 Physics of liquid crystals in cell biology. *Trends in cell biology* **32**, 140–150.
7. Saw TB, Xi W, Ladoux B, Lim CT. 2018 Biological tissues as active nematic liquid crystals. *Advanced materials* **30**, 1802579.
8. Doostmohammadi A, Ignés-Mullol J, Yeomans JM, Sagués F. 2018 Active nematics. *Nature communications* **9**, 3246.
9. Selinger JV. 2016 *Introduction to the theory of soft matter: from ideal gases to liquid crystals*. Springer.
10. Ferme LC, Ryan AQ, Haase R, Modes CD, Norden C. 2025 Timely neurogenesis drives the transition from nematic to crystalline nuclear packing during retinal morphogenesis. *Science Advances* **11**, eadu6843.
11. Andralojc H, Turley J, Weavers H, Martin P, Chenchiah IV, Bennett RR, Liverpool TB. 2025 Dynamics of Wound Closure in Living Nematic Epithelia. arXiv:cond.mat/2506.04922.
12. Faisal SM, Clewner JE, Stack B, Varela ML, Comba A, Abbud G, Motsch S, Castro MG, Lowenstein PR. 2024 Spatiotemporal insights into glioma oncostream dynamics: unraveling formation, stability, and disassembly pathways. *Advanced Science* **11**, 2309796.
13. Argento AE, Varela ML, Singh G, Visnuk DP, Jacobovitz B, Rutherford ME, Edwards MB, Chaboche Q, Orringer DA, Heth JA et al.. 2025 Gliomas organize as liquid crystals: three-dimensional nematic order, disclinations and quasi-long-range order. *bioRxiv* pp. 2025–04.
14. Selinger JV. 2024 Free Energy. In *Introduction to Topological Defects and Solitons: In Liquid Crystals, Magnets, and Related Materials* , pp. 25–39. Springer.
15. Brauns F, O'Leary M, Hernandez A, Bowick MJ, Marchetti MC. 2025 Active Solids: Defect Self-Propulsion Without Flow. arXiv:cond-mat/2502.11296.
16. Hoffmann LA, Carenza LN, Eckert J, Giomi L. 2022 Theory of defect-mediated morphogenesis. *Science advances* **8**, eabk2712.
17. Saw TB, Doostmohammadi A, Nier V, Kocgozlu L, Thampi S, Toyama Y, Marcq P, Lim CT, Yeomans JM, Ladoux B. 2017 Topological defects in epithelia govern cell death and extrusion. *Nature* **544**, 212–216.
18. Steucke KE, Win Z, Stemler TR, Walsh EE, Hall JL, Alford PW. 2017 Empirically determined vascular smooth muscle cell mechano-adaptation law. *J. Biomech. Eng.* **139**, 071005.
19. Win Z, Buksa JM, Alford PW. 2018 Architecture-dependent anisotropic hysteresis in smooth muscle cells. *Biophysical journal* **115**, 2044–2054.
20. Rothermel TM, Win Z, Alford PW. 2020 Large-deformation strain energy density function for vascular smooth muscle cells. *Journal of Biomechanics* **111**, 110005.
21. Fung Y. 1967 Elasticity of soft tissues in simple elongation. *American Journal of Physiology* **213**, 1532–1544.
22. Humphrey JD. 2003 Continuum biomechanics of soft biological tissues. *Proceedings of the Royal Society of London. Series A: Mathematical, Physical and Engineering Sciences* **459**, 3–46.
23. Gasser TC, Ogden RW, Holzapfel GA. 2006 Hyperelastic modelling of arterial layers with distributed collagen fibre orientations. *J. Royal Soc. Interface* **3**, 15–35.
24. Lai VK, Hadi MF, Tranquillo RT, Barocas VH. 2013 A multiscale approach to modeling the passive mechanical contribution of cells in tissues. *J. Biomed. Eng.* **135**, 071007.
25. Barocas VH, Tranquillo RT. 1997 An Anisotropic Biphasic Theory of Tissue-Equivalent Mechanics: The Interplay Among Cell Traction, Fibrillar Network Deformation, Fibril Alignment, and Cell Contact Guidance. *J. Biomed. Eng.* **119**, 137.
26. Zahalak GI, Wagenseil JE, Wakatsuki T, Elson EL. 2000 A cell-based constitutive relation for bio-artificial tissues. *Biophys. J.* **79**, 2369–2381.
27. Marquez JP, Genin GM, Zahalak GI, Elson EL. 2005 Thin bio-artificial tissues in plane stress: the relationship between cell and tissue strain, and an improved constitutive model. *Biophys. J.* **88**, 765–777.
28. Breuls RG, Sengers BG, Oomens CW, Bouten CV, Baaijens FP. 2002 Predicting local cell deformations in engineered tissue constructs: a multilevel finite element approach. *J. Biomech. Eng.* **124**, 198–207.
29. Taber LA. 2020 *Continuum modeling in mechanobiology* vol. 10. Springer.
30. Ben Amar M. 2025 Wrinkles, creases, and cusps in growing soft matter. *Reviews of Modern Physics* **97**, 015004.
31. Banerjee S, Gardel ML, Schwarz US. 2020 The actin cytoskeleton as an active adaptive material. *Annual review of condensed matter physics* **11**, 421–439.
32. Claussen NH, Brauns F. 2025 Mean-Field Model for Active Plastic Flow of Epithelial Tissue. *PRX Life* **3**, 023002.

33. Wool RP. 2008 Self-healing materials: a review. *Soft Matter* **4**, 400–418.
34. De Gennes PG, Prost J. 1993 *The physics of liquid crystals*. Number 83. Oxford university press.
35. Schimming CD, Viñals J. 2020 Anisotropic disclination cores in nematic liquid crystals modeled by a self-consistent molecular field theory. *Phys. Rev. E* **102**, 010701(R). (10.1103/PhysRevE.102.010701)
36. Brand HR, Pleiner H. 1994 Electrohydrodynamics of nematic liquid crystalline elastomers. *Physica A: Statistical Mechanics and its Applications* **208**, 359–372.
37. Warner M, Terentjev EM. 2007 *Liquid crystal elastomers* vol. 120. Oxford university press.
38. Tadmor EB, Miller RE, Elliott RS. 2012 *Continuum mechanics and thermodynamics: from fundamental concepts to governing equations*. Cambridge University Press.
39. Taber LA. 2004 *Nonlinear theory of elasticity: applications in biomechanics*. World Scientific.
40. Lima-Chaves GD, Acharya A, Upadhyay MV. 2025 A finite deformation theory of dislocation thermomechanics. *Journal of the Mechanics and Physics of Solids* **200**, 106141.
41. Gurtin ME, Polignone D, Viñals J. 1996 Two-phase binary fluids and immiscible fluids described by an order parameter. *Mathematical Models and Methods in Applied Sciences* **6**, 815–831.
42. Tovkach OM, Conklin C, Calderer MC, Golovaty D, Lavrentovich OD, Viñals J, Walkington NJ. 2017 Q-tensor model for electrokinetics in nematic liquid crystals. *Physical Review Fluids* **2**, 053302.
43. Beris AN, Edwards BJ. 1994 *Thermodynamics of flowing systems: with internal microstructure*. Number 36. Oxford University Press.
44. Sonnet AM, Virga EG. 2012 *Dissipative ordered fluids: theories for liquid crystals* vol. 100. Springer Science & Business Media.
45. Acharya A, Viñals J. 2020 Field dislocation mechanics and phase field crystal models. *Physical Review B* **102**, 064109.
46. Brückner BR, Nöding H, Janshoff A. 2017 Viscoelastic properties of confluent MDCK II cells obtained from force cycle experiments. *Biophysical Journal* **112**, 724–735.
47. de Gennes PG. 1975 Réflexions sur un type de polymères nématiques. *CR Acad. Sci. Ser., B* **281**, 101–103.
48. de Gennes PG. 1980 . In Helfrich W, Heppke G, editors, *Liquid Crystals of One- and Two-Dimensional Order* , p. 231. Berlin: Springer.